



1 Glacier surface mass balance modeling in the inner tropics using a
2 positive degree-day approach

3

4 **L. Maisincho^{1,2}, V. Favier³, P. Wagnon^{2,4}, V. Jomelli⁵, R. Basantes Serrano^{2,3,8},**
5 **B. Francou², M. Villacis⁶, A. Rabatel³, M. Ménégoz⁷, L. Mourre², B. Cáceres¹**

6

7

8 [1] INAMHI, Instituto Nacional de Meteorología e Hidrología, Iñaquito N36-14 y Corea,
9 Quito, Ecuador.

10 [2] IRD, Univ. Grenoble Alpes, CNRS, INPG, Laboratoire d'étude des Transferts en
11 Hydrologie et Environnement (LTHE), UMR5564, F-38000 Grenoble, France.

12 [3] Univ. Grenoble Alpes, CNRS, Laboratoire de Glaciologie et Géophysique de
13 l'Environnement (LGGE), UMR5183, F-38000 Grenoble, France.

14 [4] ICIMOD, GPO Box 3226, Kathmandu, Nepal

15 [5] Université Paris 1 Panthéon-Sorbonne, CNRS, Laboratoire de Géographie Physique
16 (LGP), 92195 Meudon, France.

17 [6] Escuela Politécnica Nacional (EPN), Ladrón de Guevara E11-253, Quito, Ecuador.

18 [7] Institut Català de Ciències del Clima (IC3), Doctor Trueta, 203 3a planta 08005
19 Barcelona (Spain)

20 [8] Universidad Regional Amazónica (IKIAM), Km 7, Via Muyuna-Atacapi, Tena, Ecuador.

21 Correspondance to: Luis Maisincho, INAMHI, Iñaquito N36-14 y Corea, Quito, Ecuador

22 lmaisincho@inamhi.gob.ec

23

24

25



26 **Abstract**

27 We present a basic ablation model combining a positive degree-day approach to
28 calculate melting and a simple equation based on wind speed to compute sublimation. The
29 model was calibrated at point scale (4,900 m a.s.l.) on Antizana Glacier 15 (0.28 km²;
30 0°28'S, 78°09'W) with data from March 2002 to August 2003 and validated with data from
31 January to November 2005. Cross validation was performed by interchanging the calibration
32 and validation periods. Optimization of the model based on the calculated surface energy
33 balance allowed degree-day factors to be retrieved for snow and ice, and suggests that
34 melting started when daily air temperature was still below 0 °C, because incoming
35 shortwave radiation was intense around noon and resulted in positive temperatures for a few
36 hours a day. The model was then distributed over the glacier and applied to the 2000-2008
37 period using meteorological inputs measured on the glacier foreland to assess to what extent
38 this approach is suitable for quantifying glacier surface mass balance in Ecuador. Results
39 showed that a model based on temperature, wind speed, and precipitation is able to
40 reproduce a large part of surface mass-balance variability of Antizana Glacier 15 even
41 though the melting factors for snow and ice may vary with time. The model performed well
42 because temperatures were significantly correlated with albedo and net shortwave radiation.
43 Because this relationship disappeared when strong winds result in mixed air in the surface
44 boundary layer, this model should not be extrapolated to other tropical regions where
45 sublimation increases during a pronounced dry season or where glaciers are located above
46 the mean freezing level.

47

48 **Keywords:** Degree-day, melting, surface mass balance, inner tropics, Antizana.



49 1 Introduction

50 Glaciers in Ecuador respond rapidly to climate change, particularly to variations in
51 temperature. The comparison of glacier extents using photogrammetric information
52 available since 1956 (Francou *et al.*, 2000) with local variations in temperature suggests that
53 local warming of the atmosphere (about 0.2 °C/decade (Vuille *et al.*, 2000)) has played an
54 important role in glacier retreat since the 1950s (Francou *et al.*, 2000), with direct
55 consequences for the local water supply to Quito (e.g., Favier *et al.*, 2008; Villacis, 2008).
56 The expected warming in the high-elevation Andes over the 21st century (between 4 °C and
57 5 °C) (Bradley *et al.*, 2006; Vuille *et al.*, 2008; Urrutia and Vuille, 2009), which is more than
58 estimated warming since the early Holocene (Jomelli *et al.*, 2011), could thus have dramatic
59 consequences for glacial retreat in Ecuador. Understanding and producing long-term models
60 of glacial retreat under local warming is thus crucial.

61 Surface mass balance models for the tropics using minimum inputs have already
62 been built and applied in the outer tropics (Kaser, 2001; Juen *et al.*, 2007) but never
63 specifically in the Ecuadorian Andes. To date, only one attempt has been made to link the
64 various energy fluxes to two input variables, monthly precipitation and temperature (Juen *et*
65 *al.*, 2007). Using a similar approach in the inner tropics makes sense because solid
66 precipitation and temperature changes have already been demonstrated to play an important
67 role in the interannual variability of ablation (Francou *et al.*, 2004). Even though the interest
68 of the positive degree-day (PDD) model is quite controversial in the tropics, where
69 temperature is generally assumed to have a limited link with the main local ablation
70 processes (Sicart *et al.*, 2008), a comprehensive test of such a model has still not been
71 performed in the inner tropics and is timely. Indeed, in the Ecuadorian Andes, air



72 temperature is known to be the main variable involved in glacier surface mass balance as it
73 controls the 0 °C level, which oscillates continuously within the ablation zone (Kaser, 2001;
74 Favier *et al.*, 2004a&b, Francou *et al.*, 2004; Rabatel *et al.*, 2013). Thus, slight changes in
75 temperature directly modify the ablation processes at the glacier surface due to the
76 precipitation phase and its impact on surface albedo (e.g., Francou *et al.*, 2004; Favier *et al.*,
77 2004a). As a consequence, during El Niño/La Niña events, atmospheric warming/cooling, or
78 more precisely the rise/drop in the 0 °C level, has major consequences for the precipitation
79 phase over the glacier, leading to high/low melting rates (e.g., Francou *et al.*, 2004; Favier *et*
80 *al.*, 2004b).

81 In this study, we developed a basic model based on variations in temperature,
82 precipitation, and wind speed to study the glacier surface mass balance on Antizana Glacier
83 15 (0.28 km²; 0°28'S, 78°09'W). Melting was assessed using a typical positive degree-day
84 approach (e.g., Braithwaite, 1995; Hock, 2003), whereas sublimation was calculated using
85 only daily wind speeds. The model was calibrated and tested on data from Antizana Glacier
86 15 (see GLACIOCLIM observatory: <http://www-lgge.ujf-grenoble.fr/ServiceObs/>) to judge
87 whether such a simple approach can reasonably quantify local glacier surface mass balance
88 and the transient snowline elevation in Ecuador.

89 **2 Study site, climatic setting and associated glaciological processes**

90 Antizana stratovolcano is one of the main ice covered summits in the Cordillera
91 Oriental of Ecuador (Figure 1). The most recent glacier inventory performed in 2014
92 showed that glaciers extended over a total surface area of 15 km² (Basantes, 2015)
93 distributed in 17 glacier tongues (Hastenrath, 1981). Glaciological and hydrological studies
94 in the area began on Antizana Glacier 15 in 1994. The glacier is located on the north-western



95 side of the volcano and is a reference site for long-term observations. The surface of the
96 glacier presently extends from 5,700 m above sea level (a.s.l.) down to 4,850 m a.s.l.

97 The study area belongs to the inner tropics, which are characterized by very low
98 temperature and moisture seasonality (e.g., Kaser and Osmaston, 2002). The low latitude
99 location yields circadian temperature variations largely exceeding those of the daily mean
100 temperature over one year. Between 2000 and 2008, the annual precipitation recorded at
101 4,550 m a.s.l. in the catchment of Antizana Glacier 15 ranged from 800 to 1,300 mm a⁻¹.
102 Precipitation was significant every month; monthly variations produced two slight maxima
103 in April and October, and slight minima in July-August and December (Favier *et al.*, 2004a).
104 As a consequence of these peculiar climatic settings, accumulation and ablation occur
105 simultaneously and continuously. The mean 0 °C level is generally close to 5,000 m a.s.l.,
106 i.e. within the ablation zone. However, this value is subject to year-to-year variability. On
107 the other hand, during the period 2000-2008, wind velocity was subject to pronounced
108 seasonal variations, with intense easterly winds generally occurring between June and
109 October (hereafter referred to as Period 1). Period 2 refers to the period from November to
110 May of the following year, which was associated with marked mass and energy losses
111 through melting (Favier *et al.*, 2004a). For instance, between 2000 and 2008, the mean wind
112 speed was 6.1 m s⁻¹ (standard deviation of daily values (STD) = 2.9 m s⁻¹) in Period 1 and
113 3.1 m s⁻¹ (STD = 2.1 m s⁻¹) in Period 2.

114 Finally, most of the local climate variability since the 1970s has been closely linked
115 to the El Niño–Southern Oscillation (ENSO) (Francou *et al.*, 2004; Vuille *et al.*, 2008).
116 There is a three month delay in the local response of the atmosphere to the ENSO signal.
117 Surface energy balance studies showed that these variations are closely linked with
118 variations in albedo that mirror changes in the precipitation phase at the glacier surface due



119 to variations in temperature.

120 **3 Data**

121 **3.1 Basic model input data**

122 **3.1.1 Daily temperature and precipitation**

123 We used data recorded at five meteorological stations and two tipping bucket rain
124 gauges (Table 1 and Figure 1). We were able to obtain a continuous homogeneous
125 temperature dataset at daily time scale from the temperature sensor of the glacier station
126 located at 4,900 m a.s.l. (hereafter referred to as AWS_{G1} , see Table 1). We filled the data
127 gaps (Table 2) by applying simple correlations between the daily temperature recorded at
128 4,900 m a.s.l. and at various neighboring stations when the stations were working
129 simultaneously (r^2 always higher than 0.75, Table 3). The stations used to fill the gaps were
130 in order of descending priority, first AWS_{M1} (installed on the lateral moraine of Glacier 15 at
131 4,900 m a.s.l.), second AWS_{G2} (installed on Glacier 15, at 5,000 m a.s.l.), when AWS_{M1} was
132 not working, third AWS_{G3} (installed on a nearby glacier, Glacier 12 at 4,900 m a.s.l.) and
133 finally AWS_{M2} (installed off-glacier at 4,785 m a.s.l.). Figure 1 and Tables 1 and 2 show the
134 location and provide additional information for each station and explain how the continuous
135 dataset from 2000 to 2008 was obtained. For AWS_{M2} and AWS_{G2} data, lapse rate corrections
136 allowed us to account for the difference in elevation between the two stations and AWS_{G1} .
137 The quality of the temperature data was checked during regular field visits conducted
138 approximately every 10 days to detect any AWS malfunction (i.e. failure of artificial
139 ventilation) and by comparing with data from the closest sensors. When data were
140 considered to be suspicious (1.2% of a total of 3,288 days) they were not used in the present



141 study.

142 Precipitation between 2000 and 2008 came from an automatic tipping bucket HOBO
143 rain gauge referred to as P4 (Figure 1) located on the moorland (*páramo*) at 4,550 m a.s.l.
144 Data from P4 were quality controlled and validated with monthly total precipitation
145 measurements at 4,550 m a.s.l. in the field using a totalizer rain gauge. When daily
146 precipitation was not available at P4 (6% of the total period), we used data from a similar
147 rain gauge hereafter referred to as P2 (Figure 1), located at 4,875 m a.s.l. The determination
148 coefficient of daily precipitation amounts between P2 and P4 was significant ($r^2 = 0.60$, $n =$
149 2,378 days, $p = 0.001$, between 2000 and 2008) even if snow precipitation occurred more
150 frequently at P2 than at P4, and snow melt in the rain gauge was delayed from a few hours
151 to maximum one day because the sensors were not artificially heated.

152 It is well known that precipitation measurements are subject to large systematic
153 errors, especially when a large proportion of precipitation falls in the form of snow in a
154 windy environment and undercatch prevails (e.g. Immerzeel *et al.*, 2012). This is the case on
155 Antizana Glacier 15. Consequently, based on a detailed analysis of measurements made with
156 a reference gauge suitable for measuring both solid and liquid precipitation (Geonor T-200b,
157 equipped with a weighing device), Wagnon *et al.* (2009) recommended applying a correction
158 factor of +51% to account for this undercatch. Given that P4 systematically collected 16.5%
159 less precipitation than the Geonor rain gauge between 2005 and 2012 (data not shown), the
160 correction factor to apply to P4 measurements was as high as +76% ($1.76 = 1.165 * 1.51$)
161 Here, we applied this correction to the precipitation at P4 between 2000 and 2008, leading to
162 a mean precipitation of 1,820 mm w.e. a^{-1} at 4,550 m a.s.l. We assumed that precipitation did
163 not vary with elevation due to the small size of the glacier (only 2 km long) (Favier *et al.*,
164 2008). Nevertheless, we did test the impact of correcting precipitation on calculations of the



165 glacier-wide climatic (or surface) mass balance (Section 6.3).

166 **3.1.2 Wind speed used to compute sublimation**

167 Turbulent heat fluxes are known to be very sensitive to wind velocity (Garratt, 1992).
168 Since on Antizana Glacier 15, the latent heat (LE) and wind speed are indeed closely
169 correlated at a daily time scale ($r = -0.79$, $n = 530$, $p = 0.001$, see Supplementary Materials,
170 Table S2), like in Favier *et al.* (2008), sublimation amounts for 2000-2008 were computed
171 using surface wind speed recorded at the same stations as temperature (see Section 3.1).
172 When wind speeds were not available (18% of a total of 3,288 days), we used daily wind
173 speed at 600 hPa available from the NCEP-NCAR Reanalysis1 (NCEP1) dataset closest to
174 Antizana volcano (77° W; 0.2° S) (Kalnay *et al.*, 1996) ($r = 0.7$ for $n = 2,685$ days with
175 data). A comparison with field data at 4,900 m a.s.l. showed that the reanalyzed wind speed
176 presented a mean bias of 0.3 m s^{-1} , which we assumed to be negligible in our surface mass
177 balance computation.

178 **3.2 Data used for model calibration and validation**

179 **3.2.1 Data used for modeling the surface energy balance**

180 The surface energy balance (SEB) was computed at 4,900 m a.s.l. for 530 days
181 between March 14, 2002 and August 31, 2003. Continuous data were available at the
182 AWS_{G1} , except between May 2 and May 6, 2002. The sensors installed on the AWS_{G1} and
183 the available data are described in Favier *et al.* (2004a&b). A second data set was used to
184 compute the surface mass balance from January 1, 2005 to November 30, 2005. Except for
185 incoming long-wave radiation, which was available only at AWS_{M1} , all the meteorological
186 variables came from AWS_{G1} . These results allowed us to calculate daily ablation, which was



187 then used as reference data to calibrate and validate the basic model. The basic model was
188 first calibrated using data from the period March 2002 to August 2003 and validated using
189 data from January to November 2005. Cross validation was then performed by interchanging
190 the calibration and validation periods.

191 Finally, the albedo measurements collected at AWS_{G1} and AWS_{G3} were used to get
192 information on surface state between 2000 and 2008 (Table 1&4). The albedo data used in
193 2006 were collected at 4,900 m a.s.l. on Antizana Glacier 12 located on the south-western
194 flank of the volcano, 3 km from Antizana Glacier 15. The slope and the aspect of the two
195 glaciers are similar and albedo was measured at the same elevation. The sensors used for
196 radiation measurements on the latter AWS were the same as those installed on AWS_{G1} .

197 **3.2.2 Glaciological data used for model validation**

198 We used the following data for model validation (Table 4):

199 1) Daily melting amounts for 43 days in 2002-2003 were obtained using “melting boxes”
200 similar to those described in Wagnon *et al.* (1999). The values used in this study are
201 those of Favier *et al.* (2004a). Melting box accuracy is hard to assess, but the
202 comparison of melting amounts from melting boxes and from surface energy balance
203 data (see Section 4.2) suggests that measured melting is generally lower, likely because
204 initial liquid water is retained by/between the small ice blocks due to capillarity. The
205 uncertainty of daily melting measured by melting boxes cannot be assessed with
206 accuracy but Favier *et al.* (2004a) observed a 30% difference between measured and
207 computed melting, suggesting the error range is likely in this order of magnitude.
208 Finally, based on the application of the surface energy balance model (Section 4.2), we
209 calculated that melting occurring below 20 cm under the surface represented 1.6 % of



- 210 total melt and was thus negligible.
- 211 2) The monthly mass balance and snow accumulation at 4,900 m a.s.l. from 2000 to 2008.
- 212 These data allowed us to assess the thickness of the snow cover and the changes in the
- 213 level of the surface due to ablation. Data from 2000 to 2003 were already used and
- 214 described by Francou *et al.* (2004).
- 215 3) The annual Antizana Glacier 15 climatic mass-balance profiles (hereafter referred to as
- 216 $b(z)$) obtained in the ablation zone from field measurements and the ELA from 2000 to
- 217 2008 (available on the GLACIOCLIM and WGMS databases). Above 5000 m a.s.l.,
- 218 Basantes Serrano *et al.* (2016) have shown that using Lliboutry's approach to interpolate
- 219 the measured data is more accurate by significantly reducing the discrepancy between
- 220 the glaciological and geodetic balance. All details regarding the glaciological
- 221 measurements and methods are described in Francou *et al.* (2004) and Basantes Serrano
- 222 *et al.* (2016).
- 223 4) The Antizana Glacier 15 glacier-wide climatic annual mass balances (B_a) from 2000 to
- 224 2008. Here we present data from Basantes Serrano *et al.* (2016), in which the glacier-
- 225 wide annual mass balance of Antizana Glacier 15 computed using the glaciological
- 226 method was recalculated using an updated delineation of the glacier and adjusted with
- 227 the geodetic method based on photogrammetric restitution of aerial photographs taken
- 228 in 1997 and 2009.
- 229 5) The annually updated hypsometry and glacier surface area of Antizana Glacier 15
- 230 computed by Basantes Serrano *et al.*, (2016). The glacier-wide annual mass balance
- 231 calculated from the basic model accounted for this revised hypsometry and area.
- 232 6) Intermittent observations and terrestrial photographs (Table 4) of the glacier surface that
- 233 were made to estimate the elevation of the transient snowline on the glacier during field



234 trips between 2004 and 2008. The daily transient snowline elevation was estimated from
235 photographs obtained with a low resolution automatic camera (Fujifilm FinePix 1400)
236 installed on the frontal moraine at 4,785 m a.s.l. These photographs were taken from the
237 location labelled “Photo” in Figure 1, and were georeferenced (Corripio, 2004). A total
238 of 712 good quality daily photographs allowed us to almost continuously monitor the
239 transient snowline elevation over time with an accuracy of ± 10 m.

240 **4 Methods**

241 **4.1 Statistical test to assess model performance**

242 To test model performance, we used the efficiency statistical test (E) proposed by
243 Nash and Sutcliffe (1970):

$$244 \quad E = 1 - (\text{RMSE}/s)^2 \quad (1)$$

245 where s is the standard deviation of the observations and RMSE is the root mean
246 squared error of the simulated variable (perfect agreement for $E=1$). The correlation between
247 measurements and model was also analyzed. Except when the p value is mentioned,
248 correlations are considered as significant if p is 0.001 or less.

249 **4.2 Surface energy balance computation**

250 At point scale (4,900 m a.s.l.), daily melting was calculated for a horizontal surface
251 by applying the classical SEB approach described in Favier *et al.* (2011), which includes
252 subglacial processes (see Supplementary Materials for details) not originally accounted for
253 in Favier *et al.* (2004a&b). Daily melting was quantified from March 14, 2003 to August 31,
254 2003 and from January 1, 2005 to November 30, 2005. Calculations were validated using
255 melting amounts measured with the melting boxes and with point mass balance measured on



256 stakes in the vicinity of the AWS_{G1} (see Supplementary Materials, Figure S2). Results using
257 Favier *et al.* (2011) approach agreed with measured melting amounts better than results in
258 Favier *et al.* (2004a&b), with a correlation coefficient of $r = 0.91$ (instead of 0.86). The
259 regression line is also closer to the 1:1 line (slope of 1.01 instead of 0.89). Over one year, the
260 heat storage below the surface is zero, and the energy excess at the surface (i.e. Q_{surface}) is
261 used to melt the snow/ice at the surface or below. As a consequence, the mean annual
262 computed melting rates only differed by 0.4% (see Supplementary Materials, Figure S1)
263 from those given by Favier *et al.* (2004a&b), suggesting that heat conduction (G) into the
264 ice/snow over one year can be disregarded. However, daily differences between the results
265 of the present study and the calculations in Favier *et al.* (2004a&b) are significant (reaching
266 20 mm w.e d^{-1} with a standard deviation of 5 mm w.e. d^{-1}) because refreezing may occur in
267 particular when sublimation is high (in Period 1) demonstrating that the use of a
268 computation scheme including G and solar radiation penetration into the ice is necessary to
269 study ablation processes at a daily timescale (e.g., Mölg *et al.*, 2008, 2009).

270 4.3 The basic model

271 4.3.1 The positive degree-day model

272 The positive degree-day model enables calculation of daily snow or ice melt $m_j(z)$ (in
273 mm w.e.) at a given elevation z (in m a.s.l.), and at time step j (in days) (Braithwaite, 1995;
274 Hock, 2003):

$$275 \quad m_j(z) = F (T_j(z_{\text{ref}}) + LR (z - z_{\text{ref}}) - T_{\text{threshold}}) \quad \text{if } T_j(z_{\text{ref}}) + LR (z - z_{\text{ref}}) > T_{\text{threshold}} \quad (2),$$

$$276 \quad m_j(z) = 0 \quad \text{if } T_j(z_{\text{ref}}) + LR (z - z_{\text{ref}}) \leq T_{\text{threshold}} \quad (3),$$

277 where F is the degree-day factor (in mm w.e. $^{\circ}\text{C}^{-1} d^{-1}$), $T_j(z)$ (in $^{\circ}\text{C}$) is the mean daily



278 temperature, $z_{\text{ref}} = 4,900$ m a.s.l. and z (in m a.s.l.) is the reference elevation and the given
 279 elevation respectively, $T_{\text{threshold}}$ (in °C) is a threshold temperature above which melting
 280 begins, and LR is the lapse rate in the atmosphere (in °C m⁻¹, hereafter expressed in °C km⁻¹
 281 for better readability). The PDD model generally assumes that $T_{\text{threshold}} = 0$ °C (van den
 282 Broeke *et al.*, 2010). However, during short periods in the daytime, melting may occur when
 283 daily mean is below 0 °C (e.g. Van den Broeke *et al.*, 2010). Here, we used $T_{\text{threshold}}$ as a
 284 calibration parameter of the model (See section 5.1).

285 The model can be run using different F values depending on the presence or absence
 286 of snow at the glacier surface at the previous time step, where $S_{j-1}(z)$ is the amount of snow
 287 in mm w.e. at the time step $j-1$:

$$288 \quad F = F_{\text{snow}} \quad \text{if} \quad S_{j-1}(z) > 0 \quad (\text{in mm w.e. } ^\circ\text{C}^{-1} \text{ d}^{-1}) \quad (4).$$

$$289 \quad F = F_{\text{ice}} \quad \text{if} \quad S_{j-1}(z) = 0 \quad (\text{in mm w.e. } ^\circ\text{C}^{-1} \text{ d}^{-1}) \quad (5).$$

290 Snow cover is the difference between ablation and snow accumulation at a given
 291 elevation z . In ablation computations, sublimation was assessed using a simple relationship
 292 based on the regression line between wind speed and sublimation (see Equation 6, Section
 293 4.3.2) like in Favier *et al.* (2008). Solid precipitation is assumed if the air temperature is
 294 below a threshold ($T_{\text{snow/rain}} = 1$ °C (Wagon *et al.*, 2009)), otherwise solid precipitation is
 295 zero. This threshold was obtained from field measurements and from direct observations of
 296 the precipitation phase in the Andes, which showed that, below this temperature, more than
 297 70% of precipitation is solid (e.g., L'hôte *et al.*, 2005). Temperature at a specific elevation z
 298 was computed assuming a constant lapse rate (LR) between the reference elevation z_{ref} ,
 299 where meteorological data are available, and z . Half-hourly field temperature measurements
 300 performed in artificially ventilated shelters at three different elevations on Antizana Glacier
 301 12 (3 km south of the Antizana Glacier 15) suggested a mean LR of -8.5 °C km⁻¹ (standard



302 deviation of $3.0 \text{ }^\circ\text{C km}^{-1}$ on half hourly values, for 18,685 values) (data not shown). This
303 vertical temperature gradient is steeper than the moist adiabatic gradient because Antizana
304 Glacier 12 and Antizana Glacier 15 are located on the leeward side of the volcano, where
305 there is a strong foehn effect whose consequence is to steepen LR (e.g., Favier *et al.*, 2004a).
306 The LR values may present a seasonal cycle, which can strongly impact the modeled glacier-
307 wide mass balance. Over one year (July 2012-July 2013), this gradient was steeper in July-
308 August (around $-9.2 \text{ }^\circ\text{C km}^{-1}$) when the wind was stronger than in the rest of the year (-8.2
309 $^\circ\text{C km}^{-1}$). We used $-8.5 \text{ }^\circ\text{C km}^{-1}$ in the present paper, and a model sensitivity test against this
310 parameter is presented in section 6 to quantify to what extent our results depend on LR
311 seasonality.

312 The elevation of the transient snowline $z_{SL,j}$, i.e. the elevation above which daily
313 snow accumulation was positive, was an output of the model and was then compared with
314 field observations. Finally, the modeled ELA is the altitude at which the annual surface mass
315 balance $b_j(z)$ is zero.

316

317 **4.3.2 Incorporating sublimation in the basic model**

318 In the tropics, sublimation is known to be an important ablation process (Winkler *et*
319 *al.*, 2009) which is worth including in a basic model. The regression line between the daily
320 wind speed and turbulent latent heat flux (see Supplementary Materials) provides the
321 equation needed to compute daily sublimation:

$$322 \quad \textit{Sublimation} = LE * 24 * 3600 / L_s = -5.73 u \quad (6)$$

323 where u is daily mean wind speed (in m.s^{-1}) and L_s is latent heat of sublimation ($L_s =$
324 $2.834 \cdot 10^6 \text{ J kg}^{-1}$).



325 Between March 2002 and August 2003, sublimation represented 3.7% of the total
326 ablation at 4,900 m a.s.l. on Antizana Glacier 15 (Favier *et al.*, 2004a). This rate may
327 increase with elevation as melting amounts decrease and wind speed increases. However,
328 because sublimation decreases with a drop in air temperature (e.g., Bergeron *et al.*, 2006),
329 sublimation is still limited at high elevations due to colder temperatures. Moreover, the
330 frequent presence of lenticular clouds on the summit of Antizana Glacier 15 suggests that
331 water condensation or re-sublimation takes place at the summit (as confirmed by frequent
332 frost deposition) and sublimation at the glacier snout likely results from the notable effect of
333 the foehn (Favier *et al.*, 2004a). The sublimation gradient is thus unclear. Because the mean
334 sublimation at 4,900 m a.s.l. was of the same magnitude ($-300 \text{ mm w.e. a}^{-1}$) as the mean
335 2000-2008 glacier-wide mass balance ($-240 \text{ mm w.e. a}^{-1}$), i.e. 15% of the glacier-wide
336 ablation ($2060 \text{ mm w.e. a}^{-1}$), assuming that sublimation is constant or decreases rapidly with
337 elevation has important consequences for the final modeled glacier-wide surface mass
338 balance. Since the gradient of sublimation as a function of altitude is not yet available from
339 SEB modelling, we developed rough hypotheses for its distribution with elevation. In this
340 study, the sublimation gradient was assumed to be equal to 0 (constant sublimation), but a
341 sensitivity test was performed (Section 6.3) using a linear decrease until zero was reached at
342 the summit where frost may result in insignificant sublimation.

343 **5 Model calibration and validation at point scale**

344 **5.1 Calibration over the 2002-2003 period**

345 When running the model at point scale (4,900 m a.s.l., i.e. the elevation of the input
346 data), LR can be discarded and only three parameters F_{snow} , F_{ice} and $T_{\text{threshold}}$ need to be



347 calibrated. $T_{\text{threshold}}$ was first obtained as the zero melting intercept given by the regression
348 line between daily temperature and daily melting from March 14, 2002 to August 31, 2003
349 ($T_{\text{threshold}} = -2.05^{\circ}\text{C}$). The basic model was trained over 2002-2003 period using ablation
350 computed from the SEB approach (hereafter referred to as ‘SEB ablation’). We
351 distinguished days with snow at the surface from days without (bare ice) using a separation
352 according to a threshold ($a_{\text{threshold}}$) applied on measured surface albedo. Optimization of this
353 threshold allowed us to calibrate the F_{snow} value only in the presence of snow cover and F_{ice}
354 only in the case of bare ice. This value is not a parameter of the PDD model, since it is not
355 used when the model computes the surface state (snow or ice).

356 We then multiplied the mean daily temperature by the corresponding F value and
357 added the daily sublimation computed with Equation (7). The resulting ablation is hereafter
358 referred to as ‘T/ablation’.

359 Model calibration was performed using a Monte-Carlo approach based on 1,000,000
360 simulations to obtain the best calibration parameters, i.e. the degree-day factors (F_{ice} and
361 F_{snow}) in equation (2) and the albedo threshold ($a_{\text{threshold}}$). The basic model was optimized at
362 a daily time scale and the best score ($r = 0.81$; $\text{RMSE} = 6.5 \text{ mm w.e. d}^{-1}$, $E = 0.64$) was
363 obtained for $F_{\text{snow}} = 5.68 \text{ mm w.e. }^{\circ}\text{C}^{-1} \text{ d}^{-1}$, $F_{\text{ice}} = 10.53 \text{ mm w.e. }^{\circ}\text{C}^{-1} \text{ d}^{-1}$ and $a_{\text{threshold}} = 0.49$.
364 The latter threshold is consistent with field observations (Figure 2).

365 Logically, the cumulative ablation obtained with the basic model (11.0 m w.e) is
366 similar but slightly lower than the value given by the full energy balance model (11.3 m
367 w.e.) and the melting obtained with the basic model was indeed highly correlated with that
368 derived from the SEB equation. More instructively, the annual ablation cycle was accurately
369 reproduced (Figure 3a – red line) with reduced ablation during windy periods and increased
370 ablation when the wind speed is low. As a consequence, once the respective degree-day



371 factors were accurately calibrated, the model was able to correctly reproduce the seasonal
372 variability of ablation.

373 **5.2 Validation using the year 2005**

374 To validate the model, we applied it to the year 2005 period using parameters
375 optimized over the 2002-2003 period (Figure 3b – red line). Even though the cumulative
376 ablation obtained with the basic model (6.7 m w.e from January 1 to November 30 2005)
377 was slightly overestimated compared with that from the full energy balance model (5.8 m
378 w.e.), the scores ($r = 0.81$, $n = 334$, $p = 0.001$, $RMSE = 6.5 \text{ mm w.e. d}^{-1}$, $E=0.57$) were
379 acceptable, which gave us confidence in the ability of the model to reproduce melting and
380 ablation.

381 **5.3 Cross validation of the model**

382 To assess the impact of the choice of the calibration period on the accuracy of model
383 parameters and in turn, on model results, the periods 2002-03 and 2005 were interchanged
384 and used as validation and calibration periods, respectively (Figure 3 – blue lines). This
385 time, the zero melting intercept is obtained with $T_{\text{threshold}} = -2.14 \text{ }^{\circ}\text{C}$, and the best score ($r =$
386 0.84 ; $RMSE = 5.5 \text{ mm w.e. d}^{-1}$, $E = 0.69$) was obtained for $F_{\text{snow}} = 4.24 \text{ mm w.e. }^{\circ}\text{C}^{-1} \text{ d}^{-1}$,
387 $F_{\text{ice}} = 9.45 \text{ mm w.e. }^{\circ}\text{C}^{-1} \text{ d}^{-1}$ and $a_{\text{threshold}} = 0.56$, which is not very different from the original
388 parameters. This time, the cumulative ablation obtained for the validation period with the
389 basic model (10.4 m w.e from March 14, 2002 to August 31, 2003) was slightly
390 underestimated compared with that from the full energy balance model (11.3 m w.e.).
391 Nevertheless, the scores ($r = 0.8$, $n = 334$, $p = 0.001$, $RMSE = 6.8 \text{ mm w.e. d}^{-1}$, $E=0.62$)
392 remained acceptable which confirmed our confidence in the model.



393 **5.4 Validation with ablation stakes**

394 An in-depth analysis of the model was performed at 4,900 m a.s.l. The model was
395 run using the mean daily temperature and wind speed recorded from 2000 to 2008 at 4,900
396 m a.s.l. The separation between snow and ice was not based on albedo values, but directly
397 from the computed presence of snow at the surface. The results were consequently
398 independent of $a_{\text{threshold}}$. Surface ablation was computed using the calibration described in
399 section 5.1 between March 14, 2002 and August 31, 2003, whereas the calibration described
400 in Section 5.3 was preferred in 2005 (January 1 to November 30, 2005). For the other
401 periods, the calibrated parameters in 2002-03 and 2005 were averaged ($F_{\text{snow}} = 4.96$ mm w.e.
402 $^{\circ}\text{C}^{-1} \text{d}^{-1}$, $F_{\text{ice}} = 9.99$ mm w.e. $^{\circ}\text{C}^{-1} \text{d}^{-1}$, $T_{\text{threshold}} = -2.09^{\circ}\text{C}$).

403 The results showed that the model accurately reproduced well the cumulative glacier
404 mass balance at 4,900 m a.s.l. (Figure 4). In particular, the moderate ablation from 2000-
405 2001 and 2008 was clearly reproduced. This suggests that the model accurately
406 distinguished the surface states and accurately computed accumulation and ablation. Finally,
407 using the mean calibration described in the previous paragraph, we observed that the model
408 worked perfectly for the period 2000-2008.

409 **5.5 Validation of mean coefficients with melting boxes**

410 The model was applied using the set of mean parameters described in section 5.4,
411 and the resulting daily melting values were compared with the melting amounts collected by
412 the melting boxes over a period of 43 days. The surface states used to calculate melting were
413 those identified in the field, giving a more accurate validation of melting amounts according
414 to the real surface state. The correlation between modeled and measured daily melting was



415 significant ($r = 0.8$; $n = 43$; $p = 0.001$), but the mean modeled melting rate was higher (22.9
416 mm w.e. d^{-1}) than observations (15.6 mm w.e. d^{-1}), because the slope of the regression line
417 between observed and modeled melting was 1.05. This discrepancy is likely explained by
418 the water retained in the melting boxes that leads to underestimation of the actual melting
419 amounts. Indeed, the mean melting rate computed from the SEB approach (19.4 mm w.e. d^{-1})
420 was closer to the results of the basic model.

421 **5.6 Final validation and model parameterization used in this study**

422 The calibrated parameters in 2002-03 and 2005 were averaged ($F_{\text{snow}} = 4.96$ mm w.e.
423 $^{\circ}\text{C}^{-1} d^{-1}$, $F_{\text{ice}} = 9.99$ mm w.e. $^{\circ}\text{C}^{-1} d^{-1}$, $T_{\text{threshold}} = -2.09^{\circ}\text{C}$). Averaging albedo threshold values
424 ($a_{\text{threshold}} = 0.525$), also allowed us to assess the uncertainty of the model compared to the
425 surface energy balance model in 2002-03 and 2005. We observed that the model keeps a
426 good score while using these averaged parameters (Table 5 and Figure 3 – green lines). The
427 cumulative ablation obtained with the basic model was slightly underestimated for the
428 period 2002-2003 (10.7 m w.e.) and slightly overestimated for 2005 (6.4 m w.e), but
429 logically, the biases were then reduced for both periods.

430 In the following sections, we describe how the model was applied using this final set
431 of averaged parameters, and how model uncertainty was tested using the parameters
432 obtained by each calibration separately.

433 **6 Model validation at glacier scale**

434 The model was applied at 25 m intervals in the elevation range using the mean daily
435 temperature and wind speed recorded from 2000 to 2008 at 4,900 m a.s.l. To assess the



436 accuracy of the model and review its parameterizations, a sensitivity test of the computed
437 surface mass balance was performed on the main model parameters (Table 6): the
438 temperature threshold, the degree-day factors for ice and snow, and the temperature lapse
439 rate (LR). We tested the uncertainty of the optimal degree-day factors and $T_{\text{threshold}}$ linked to
440 the choice of $a_{\text{threshold}}$. The assumptions concerning sublimation and precipitation
441 distributions with elevation were also tested.

442

443 **6.1 Modeling the distributed surface mass balance over the period 2000-2008**

444 We checked whether our basic model was able to properly reproduce 1) the temporal
445 and 2) spatial variability of the surface mass balance of Antizana Glacier 15. The model was
446 run using mean daily temperature, wind speed, and precipitation recorded at 4,900 m a.s.l.
447 on the glacier from 2000 to 2008, using the parameter set described in section 5.6. We
448 assumed that sublimation was constant with elevation. The resulting mass balances were
449 compared with the measurements of the surface mass balance (b_a) made on the glacier.

450 Overall, simulated and measured vertical mass balance $b(z)$ agreed fairly well in the
451 ablation zone (Figure 5), even though in 2002-2003, the mass balance gradient with
452 elevation was too steep between 4900 m a.s.l and 5000 m a.s.l.. However, in the upper part
453 of the glacier, the point mass balance (accumulation) was generally overestimated (see
454 Section 7.4).

455 Compared with the other years, the performance of the model was rather weak in
456 2002-2003 and in 2005. One peculiarity of this 2002-03 hydrological year was that the
457 albedo was particularly low over both snow covered surfaces and bare ice (Figure 6). This
458 suggests that the snow and ice were frequently dirty. Indeed, albedo measurements made in



459 the ablation zone of Antizana Glaciers 15 and Glacier 12 between 2000 and 2008 were often
460 below 0.3 for the ice and rarely above 0.56 for snow (Figure 6). We consequently decided to
461 re-run the model using the parameters described in section 5.1 for 2002-03 (respectively
462 described in section 5.3 for 2005). The performance of the model was improved in the
463 ablation zone suggesting that the parameters described in section 5.1 are suitable for years
464 with dirty ice (i.e. 2002 and 2003) but are likely too high for years when the ice is cleaner.
465 Conversely, the parameters described in section 5.3 are suitable for years with clean ice.

466 We also compared our modeled glacier-wide climatic mass balance with mass
467 balance estimates in Basantes Serrano *et al.* (2016) (Figure 7). Results were in good
468 agreement with Basantes Serrano's estimates, and even better ($r^2 = 0.87$, $p = 0.001$, RMSE =
469 $0.29 \text{ m w.e. a}^{-1}$) when we used the optimized parameters obtained in section 5.1 (and in
470 section 5.3) for the year 2002-2003 (and for 2005, respectively). In this case, the mean
471 modeled mass balance between 2000 and 2008 ($0.06 \text{ m w.e. a}^{-1}$) was slightly more positive
472 than the mean observed geodetic mass balance ($-0.12 \text{ m w.e. a}^{-1}$) for 2000-2008 (Figure 7a).
473 However, when we only used the parameters given in section 5.6 the mean modeled mass
474 balance between 2000 and 2008 ($0.08 \text{ m w.e. a}^{-1}$) was still closer to field observations ($r^2 =$
475 0.78 , $p = 0.001$).

476 **6.2 Modeling the transient snowline and ELA variations**

477 To further validate the model, we compared the modeled vs. measured annual ELA,
478 and the modeled vs. measured transient snowline at a daily time step. The modeled and
479 measured transient snowline elevations were averaged over 15 days to reduce the impact of
480 precipitation uncertainty on model results and to improve the readability of the figure.
481 Indeed, because the tipping bucket rain gauges are not artificially heated, the snow can



482 accumulate inside the funnel and only melt several hours or even a day after the
483 precipitation occurred. This can lead to some shifts in the modeled daily transient snowline
484 time series.

485 The modeled snowline was in good agreement with the observed measured transient
486 snowline ($r = 0.69$, $n = 96$, $p = 0.001$ for 15-day periods between 2004 and 2008 and $r =$
487 0.70 , $n = 712$, $p = 0.001$, based on daily values) demonstrating that the model was able to
488 reproduce the altitudinal distribution of accumulation and ablation at a short time scale
489 (Figure 8a&b). The difference between the modeled and the measured transient snowline
490 was small (45 m (standard deviation STD = 47 m) for 15-day average snowlines and 30 m
491 (STD = 59 m) for the daily snowlines (712 observations)). The modeled annual ELA also
492 matched the measured ELA well ($r^2 = 0.83$, $n = 9$ years, $p = 0.003$, RMSE = 19 m), as a
493 direct consequence of the good agreement between the modeled and the observed transient
494 snowlines.

495 **6.3 Model sensitivity**

496 A sensitivity test was performed on every model parameter (F_{ice} , F_{snow} , $T_{threshold}$ and
497 LR), on the gradient of sublimation as a function of altitude as well as of precipitation
498 amounts (Table 6). We also tested the way the degree-day factor and threshold temperature
499 were impacted by the choice of $a_{threshold}$ (Table 5), showing that the model parameters
500 described in Section 5.6 were close to those obtained with the best calibration of $a_{threshold}$ for
501 both 2002-2003 and 2005. This suggests that calibration is not very sensitive to $a_{threshold}$. As
502 is always the case with PDD models (e.g. Azam *et al.*, 2012), the results are sensitive to LR ,
503 degree-day factors, and temperature threshold. These parameters are actually inter-
504 dependent and different parameter sets could thus provide similar results. The results are



505 also very sensitive to the amount and distribution of precipitation over the glacier area. This
506 analysis showed that without applying a +76% correction for precipitation, as suggested by
507 Wagnon *et al.* (2009), the agreement between simulated and measured mass balance would
508 have been much worse. In conclusion, this basic model is able to properly simulate the mass
509 change and the melting of Antizana Glacier 15 provided that it is thoroughly calibrated using
510 a substantial dataset, which is a prerequisite for such modeling. This study suggests that in-
511 situ measurements tend to underestimate precipitation amounts (strong undercatch of snow,
512 especially when the weather is windy), and a significant correction is needed to assess real
513 precipitation.

514 **7 Discussion**

515 **7.1 On the existing relationship between T and energy fluxes**

516 To understand which physical processes are responsible for the good performance of
517 this basic model, we compared the basic model melting amounts (hereafter referred to as
518 T/melting) with the different energy fluxes recorded at AWS_{GI}. A significant correlation was
519 found between the T/melting and the net shortwave radiation S ($r = 0.71$, $n = 530$ days, $p =$
520 0.001). A moving correlation coefficient (r) between S and the T/melting over 30 days
521 revealed variations over the annual cycle but the coefficient was generally 0.8 when
522 temperatures underwent significant variations over a period of one month (data not shown).
523 However, the correlation decreased when there was no variation in temperature over a
524 longer period.

525 An in-depth analysis of correlations between daily energy fluxes and temperature
526 (see Supplementary Materials) revealed moderate but significant (at $p = 0.001$) correlations



527 between air temperature, S or albedo, and incoming shortwave radiation but only during
528 periods with low speed winds. Since melting amounts during those periods (Period 2 and
529 Period 1 with $u < 4 \text{ m s}^{-1}$) represented more than 73% of the total melting amounts over the
530 study period (i.e. 11.3 m w.e. between March 14, 2002 and August 31, 2003), the
531 relationship between T and S likely largely explains the link between ablation and T .

532 The constant temperate conditions are always close to melting, and any slight
533 increase in the incoming energy will enhance melting. As a consequence, any small change
534 in T may have important consequences for precipitation phase, albedo, S and finally for
535 melting. However, the relationship with S_{\downarrow} only exists when the wind speed is low.
536 Consequently, the model performance is likely to decrease when the wind becomes stronger.
537 In our case, this had limited effects on melting on Antizana Glacier 15, since the windy
538 periods were also low-melting periods, and as a consequence, had no significant impact on
539 total melting amounts.

540 **7.2 On the accuracy of model parameterization**

541 **7.2.1 Glacier slope and aspect**

542 Several studies have shown that degree-day factors vary according to the slope and
543 aspect of a glacier (e.g., Vincent *and* Six., 2013). Here, the basic model calibration was
544 performed using results from surface energy balance calculations for a horizontal surface
545 whereas the glacier ablation area presents a mean slope of 28° and is oriented NW. Based on
546 the characteristics of the ablation zone, the best score of the basic model calibration would
547 decrease ($r = 0.56$, $p = 0.001$, $E = 0.31$ for 2002-2003) if we account for a 28° slope facing
548 NW, suggesting that these calibration values at a daily time scale are only suitable for a



549 horizontal surface. However, the impact is more limited at monthly and annual time scales,
550 because the glacier is located at the latitude of 0° and there are fewer seasonal variations in
551 melting caused by changes in the solar zenith angle than at other latitudes. Thus, the
552 difference between annual ablation for a horizontal surface and for the mean slope and
553 aspect of the ablation zone was less than 7% over 18 months. Nevertheless, it may be
554 preferable to use the basic model to assess glacier ablation for horizontal surfaces.

555 **7.2.2 $T_{\text{threshold}}$**

556 Model parameterization suggests that melting began when the daily temperature was
557 below 0°C . First, using results from the surface energy balance model, we analyzed the
558 frequency of melting events that occurred when the mean daily temperature was negative.
559 We found that, (except for 4 days), melting was always significant, even when daily
560 temperature was equal to -1.7°C , but nil at -2.1°C , which was the lowest daily temperature
561 recorded in 2002-2003 and 2005. Observations made with melting boxes also showed that
562 out of the 43 days of direct field observations, melting amounts were always significant,
563 even if the mean daily air temperature was below 0°C on nine days. For example, a daily
564 melt of $3.8\text{ mm w.e. d}^{-1}$ on July 31, 2002 was measured when the mean daily air temperature
565 was -1.3°C .

566 The same situation has already been observed in Greenland (Van den Broeke *et al.*,
567 2010), where a -5°C threshold was necessary to remove modeling biases caused by the
568 occurrence of short periods of melting when significant nocturnal refreezing occurred.
569 Indeed, these periods were characterized by mean daily air temperatures below 0°C due in
570 particular to unbalanced longwave budgets at night, but also by major incoming shortwave
571 radiation leading to diurnal melting.



572 **7.2.3 Albedo threshold**

573 The optimal albedo threshold between ice and snow surfaces was rather low
574 compared to values reported in the literature (e.g., Oerlemans *et al.*, 2009). The snow cover
575 was generally thin because permanent snow is very rare at 4,900 m a.s.l. on Antizana
576 (Wagnon *et al.*, 2009). This suggests that the ice below the surface snow cover may impact
577 albedo measurements. The patchy distribution of snow on the surface of the glacier caused
578 by the high winds on Antizana (Wagnon *et al.*, 2009) may also explain the low values.
579 Indeed, even when thin snow still covers the surface of the glacier, snow may not be present
580 everywhere. In such a case, the exposed ice surfaces may impact the mean albedo values.

581 **7.3 Degree-day factors F**

582 When we compared the F values from other regions, we found that our calibrations
583 ($F_{\text{snow}} = 4.96$ mm w.e. $^{\circ}\text{C}^{-1} \text{d}^{-1}$, $F_{\text{ice}} = 9.99$ mm w.e. $^{\circ}\text{C}^{-1} \text{d}^{-1}$ from section 5.6) were close to
584 those obtained in the sub-tropical zone, for instance at Chhota Shigri Glacier (32.28°N,
585 77.58°E, $F_{\text{snow}} = 5.28$ mm w.e. $^{\circ}\text{C}^{-1} \text{d}^{-1}$, $F_{\text{ice}} = 8.63$ mm w.e. $^{\circ}\text{C}^{-1} \text{d}^{-1}$) (Azam *et al.*, 2014).
586 However, they are also similar to those observed Storbreven in Norway (61.57°N 8.13°E,
587 $F_{\text{snow}} = 4.9$ mm w.e. $^{\circ}\text{C}^{-1} \text{d}^{-1}$, $F_{\text{ice}} = 8.5$ mm w.e. $^{\circ}\text{C}^{-1} \text{d}^{-1}$) or Svartisheibreen in Norway
588 (66.58°N, 13.75°E, $F_{\text{snow}} = 6.0$ mm w.e. $^{\circ}\text{C}^{-1} \text{d}^{-1}$, $F_{\text{ice}} = 9.8$ mm w.e. $^{\circ}\text{C}^{-1} \text{d}^{-1}$) (Radic and
589 Hock, 2011).

590 **7.4 Model accuracy in the accumulation zone**

591 Accumulation data on Antizana Glacier 15 are currently poorly reliable. Using the
592 precipitation correction proposed by Wagnon *et al.* (2009), we observed that the simulated
593 and measured vertical mass balance $b(z)$ agreed at low elevations, but not in the



594 accumulation zone (Figure 5).

595 Nevertheless, Basantes Serrano *et al.* (2016) adjusted the mass balance series of
596 glacier 15 with the 1997-2009 geodetic mass balance. The two matched only if the original
597 accumulation measurements were systematically underestimated by a factor of 60%, due to
598 the difficulty in recognizing a year-to-year reference level inside the snow during field
599 observations, leading to sometimes erroneous in-situ accumulation measurements. This
600 suggests that a correction factor should be applied to accumulation measurements given by
601 Francou *et al.* (2004). Except for 2000, where this assumption yields a peculiar shape of
602 modeled accumulation above 5000 m a.s.l., and for 2002 where accumulation was still
603 underestimated, this assumption yields better agreement between modeled and observed
604 mass balance at any elevation (Figure 5). This confirms that accumulation was largely
605 underestimated by field measurements.

606 **7.5 Temporal variation in degree-day factors**

607 We observed that the quality of the model in the ablation zone was improved if the
608 model was applied with different parameters in 2002-2003 and in 2005 than the parameters
609 used in other years. This suggests that our optimized parameters may vary depending on the
610 period of time (e.g., Huss and Bauder, 2009) reflecting variations in albedo (since degree-
611 day factors for ice differ with the state of the surface).

612 For past or future climate reconstructions, given that degree-day factors may vary as
613 a function of time, the uncertainty range of F values should always be taken into
614 consideration when assessing the final uncertainty of the results. El Niño events are
615 characterized by enhanced melting, partly due to low-albedo conditions (Francou *et al.*,
616 2004), whereas the opposite situation is observed during La Niña events. Consequently,



617 using different F values for the two events is highly recommended, irrespective of whether
618 the goal of the study is to reconstruct past ablation or to make future projections.

619 **7.6 Accuracy of the modeled transient snowline**

620 Overall, there was a good agreement between the modeled and measured transient
621 snowline, suggesting that even though the model is not physically based, it is able to broadly
622 simulate most of the important physical processes controlling the surface mass balance of
623 the glacier, or the transient snowline, likely because the 0 °C level, which has a direct impact
624 on the precipitation phase (snow or rain) is a key variable governing the mass change of this
625 glacier (e.g., Favier *et al.*, 2004a&b, Francou *et al.*, 2004). Nevertheless, in 2008, the
626 differences between the 15-day average of the modeled and observed transient snowlines
627 were larger than during the rest of the study period. These differences are likely due to either
628 inaccurate observations of the snowlines due to some failures of the automatic camera, or
629 the exceptional variability of the snowline in 2008 (Figure 8b). Indeed, during camera
630 breakdowns, the 15-day snow line elevation was obtained from photographs taken during
631 field trips. But such trips were conducted once or twice every 15 days, and as a
632 consequence, the 15-day average only corresponded to 1 or 2 observations that were
633 possibly not representative of the 15-day period. In addition, the simulated snowline
634 sometimes varied considerably from day to day, which was less visible for the observed
635 snowline (Figure 8b). This marked variability is probably due to recurrent small snow falls
636 over an icy surface, a situation in which the model is very sensitive to precipitation
637 uncertainties. Indeed, if solid precipitation is underestimated, snowfalls are not large enough
638 to durably cover the glacier surface, leading to large day-to-day variability of the snowline
639 elevation, although in reality, the glacier is mostly snow covered. On the contrary, if solid



640 precipitation is overestimated, some simulated snowfalls may artificially shift the snowline
641 to lower elevations than in reality while the glacier may be mostly free of snow.

642 **8 Conclusion**

643 The good agreement between temperature and glacier ablation or mass balance is not
644 fortuitous but based on similar relationships as those found at other latitudes. Despite the
645 limited variation in annual temperature (less than 3.5 °C, based on daily means), our study
646 revealed a significant correlation between daily temperature and melting if a distinction
647 between ice and snow was made, and provided that the model parameters (F_{ice} , F_{snow} ,
648 $T_{threshold}$, LR) were correctly calibrated. The comparison between daily temperature and the
649 energy fluxes demonstrated that both air temperature and surface melting were closely
650 linked to the net shortwave radiation budget through the impact of the albedo, which is
651 mainly controlled by the precipitation phase (Favier *et al*, 2004a). However, we observed
652 that the relationship between temperature and incoming shortwave radiation disappeared
653 when the wind speed was high.

654 Moreover, despite the often weak correlations between incoming heat fluxes and
655 temperature, a basic model including simple sublimation estimation, applied to local data
656 gave accurate results on Antizana Glacier 15. The model is also suitable for the estimation of
657 the transient snowline and ELA.

658 Because the correlation between temperature and melting is less significant with high
659 speed winds, this type of model should not be used in the case of high sublimation (i.e.
660 windy periods). However, in the case of Antizana Glacier 15, the consequences were limited
661 for the mean monthly ablation because high sublimation events generally occurred when the
662 temperature and melting (and in turn ablation since melting is the main ablation process



663 here) on the glacier were low. This study showed that variations in the annual mass balance
664 were well reproduced when the temperature was accurately assessed and when the model
665 enabled correct estimation of the surface state (i.e. indirect estimation of surface albedo).
666 However, full SEB computation reproduces measured ablation better, demonstrating that a
667 complete surface energy balance model is preferable when accurate incoming fluxes are
668 available (see Supplementary Materials, Figure S2). Several results also suggest that melting
669 began when the daily mean air temperature 2 m above the surface of the glacier was still
670 below 0 °C. If a threshold below 0 °C for temperature is not accounted for, a new calibration
671 of the degree-day factors and the temperature lapse rate would be needed, which would lead
672 to higher degree-day factors and/or a steeper temperature gradient.

673 In spite of the fairly good results we obtained, the model should be used with caution
674 at high elevations where ablation is reduced, and when the wind speed is high. However, this
675 study goes one step further in demonstrating the high sensitivity of glaciers to temperature
676 changes in Ecuador. The Antizana glaciers have lost more than 30% of their area since 1950
677 (Francou *et al.*, 2000; Rabatel *et al.*, 2013), and temperatures in the tropical Andes have
678 increased by up to 0.68 °C since 1939 (Vuille *et al.*, 2008). Because several studies suggest
679 that atmospheric warming will accelerate in the future and may reach 5 °C at the end of the
680 21st century (e.g., Vuille *et al.*, 2008; Urrutia and Vuille, 2009), the ELA may rise 600 m and
681 reach almost the elevation of the summit of Antizana. In these conditions, Antizana glaciers
682 might drastically shrink or even disappear, which will have major consequences for local
683 water supplies. Knowing the exact range of expected future temperature changes is thus
684 crucial to assess its impact on local water resources.

685 **Acknowledgments**

686 This work was supported by IRD (French Research Institute for Development), in



687 collaboration with the INAMHI (*Instituto Nacional de Meteorología e Hidrología*), the
688 EPMAPS (*Empresa Pública Metropolitana de Agua Potable y Saneamiento de Quito*), and
689 the EPN (*Escuela Politécnica Nacional de Quito*), the IRD program LMI- GREATICE, the
690 French *Service National d'Observation* GLACIOCLIM, JEAI-IMAGE and SENESCYT-
691 EPN PIC-08-506. M.L. Maisincho is grateful to AIRD for providing financial support for his
692 PhD. We thank INAMHI and EPN for providing the meteorological data from Izobamba and
693 Quito station respectively. Reanalyzed data were provided by the NOAA/OAR/ESRL PSD,
694 Boulder, Colorado, USA, from their Web site at <http://www.esrl.noaa.gov/psd/>. Special
695 thanks to Marlon Calispa (EPN), Juan Carvajal and Ricardo Felix (INAMHI) for support in
696 the office and in the field, sometimes in harsh conditions. This work was supported by a
697 grant from LABEX OSUG@2020 (*Investissements d'avenir – ANR10 LABX56*). We also
698 thank the two anonymous reviewers of the first version of this paper and Mauri Pelto for
699 their relevant comments.



700 **References**

- 701 Azam, M. F., Wagnon, P., Ramanathan, A., Vincent, C., Sharma, P., Arnaud, Y., & Berthier,
702 E. From balance to imbalance: a shift in the dynamic behaviour of Chhota Shigri
703 glacier, western Himalaya, India. *Journal of Glaciology*, 58(208), 315-324, 2012.
- 704 Azam, M.F., Wagnon, P., Vincent, C., Ramanathan, A., Linda, A., and Singh, V.B.:
705 Reconstruction of the annual mass balance of Chhota Shigri glacier, Western
706 Himalaya, India, since 1969, *Annals of Glaciology* 55(66), doi:
707 10.3189/2014AoG66A104, 2014.
- 708 Basantes, R., Contribution à l'étude de l'évolution des glaciers et du changement climatique
709 dans les Andes équatoriennes depuis les années 1950, PhD Thesis, Univ. De
710 Grenoble, Grenoble, France, 207pp., 2015.
- 711 Basantes Serrano, R., Rabatel, A., Francou, B., Vincent, C., Maisincho, L., Cáceres, B.,
712 Galarraga, R., and Alvarez, D.: Slight mass loss revealed by reanalyzing glacier mass
713 balance observations on Glaciar Antisana 15 α (inner tropics) during the 1995-2012
714 period, *Journal of Glaciology*, 2016, doi: 10.1017/jog.2016.17.
- 715 Bergeron, V., Berger, C., and Betterton, M. D.: Controlled irradiative formation of penitents,
716 *Phys. Rev. Lett.*, 96, 098502, doi: 10.1103/PhysRevLett.96.098502, 2006.
- 717 Bradley, R.S., Vuille, M., Diaz, H.F., and Vergara, W.: Threats to water supplies in the
718 Tropical Andes. *Science*, 312, 5781, 1755-1756, 2006.
- 719 Braithwaite, R.J.: Positive degree-day factors for ablation on the Greenland ice-sheet studied
720 by energy balance modeling, *J. of Glaciol.*, 41(137), 153-160, 1995.
- 721 Cáceres, B., Francou, B., Favier, V., et al.: Glacier 15, Antisana, Ecuador: its glaciology and
722 relations to water resources. In: Demuth, S., A. Gustard, E. Planos, F. Scatena and E.



- 723 Servat (Eds.), *Climate Variability and Change—Hydrological Impacts*. Proceedings
724 of the Fifth FRIEND World Conference held at Havana, Cuba, November 2006,
725 IAHS Publ. 308, 479–482, 2006.
- 726 Corripio, J.: Snow surface albedo estimation using terrestrial photography, *Int. J. Remote*
727 *Sens.*, 25, 5705–5729, doi:10.1080/01431160410001709002, 2004.
- 728 Favier, V., Wagnon, P., and Ribstein, P.: Glaciers of the outer and inner tropics: a different
729 behavior but a common response to climatic forcing. *Geophys. Res. Lett.*, 31,
730 L16403. doi:10.1029/2004GL020654, 2004.
- 731 Favier, V., Wagnon, P., Chazarin, J.-P., Maisincho, L., and Coudrain, A.: One-year
732 measurements of surface heat budget on the ablation zone of Antizana glacier 15,
733 Ecuadorian Andes. *J. Geophys. Res.*, 109, D18105. doi:10.1029/2003JD004359,
734 2004b.
- 735 Favier, V., Coudrain, A., Cadier, E., Francou, B., Ayabaca, E., Maisincho, L., Praderio, E.,
736 Villacis, M., and Wagnon, P.: Evidence of groundwater flow on Antizana ice-covered
737 volcano, Ecuador, *Hydrolog. Sci. J.*, 53(1), 278–291, 2008.
- 738 Favier, V., Agosta, C., Genthon, C., Arnaud, L., Trouvillez, A., and Gallée, H.: Modeling the
739 mass and surface heat budgets in a coastal blue ice area of Adelie Land, Antarctica, *J.*
740 *Geophys. Res.*, 116, F03017, doi:10.1029/2010JF001939, 2011.
- 741 Francou, B., Ramírez, E., Cáceres, B., and Mendoza, J.: Glacier Evolution in the Tropical
742 Andes During the Last Decades of the 20th Century: Chacaltaya, Bolivia, and
743 Antizana, Ecuador, *Ambio*, 29, 416–422, 2000.
- 744 Francou, B., Vuille, M., Favier, V., and Cáceres, B.: New evidence for an ENSO impact on
745 low latitude glaciers: Antizana 15, Andes of Ecuador, 0°28'S. *J. Geophys. Res.*, 109,
746 D18106, doi:10.1029/2003JD004484, 2004.



- 747 Garratt, J. R.: The atmospheric boundary layer, Cambridge, Cambridge University Press,
748 316 pp., 1992.
- 749 Hastenrath, S.: The glaciation of the Ecuadorian Andes, Balkema, 173 pp., 1981.
- 750 Hock, R.: Temperature index melt modelling in mountain areas, *J. Hydrol.*, 282(1-4), 104-
751 115, doi: 10.1016/S0022-1694(03)00257-9, 2003.
- 752 Huss M., and Bauder, A.: 20th-century climate change inferred from four long-term point
753 observations of seasonal mass balance. *Ann. Glaciol.*, 50, 207-214, 2009.
- 754 Immerzeel, W.W., Pellicciotti, F., and Shrestha, AB: Glaciers as a proxy to quantify the
755 spatial distribution of precipitation in the Hunza basin. *Mt. Res. Dev.*, **32**(1), 30–38,
756 doi: 10.1659/MRDJOURNAL- D-11-00097.1, 2012.
- 757 Jomelli, V., Khodri, M., Favier, V., Brunstein, D., Ledru, M.P., Wagnon, P., Blard, P.H.,
758 Sicart, J.E., Braucher, R., Grancher, D., Bourlès, D., and Vuille, M.: Irregular
759 tropical glacier retreat over the Holocene driven by progressive warming, *Nature*,
760 474, 196-199, doi:10.1038/nature10150, 2011.
- 761 Jordan, E., Ungerechts, L., Caceres, B., Penafiel, A., and Francou, B.: Estimation by
762 photogrammetry of the glacier recession on the Cotopaxi Volcano (Ecuador) between
763 1956 and 1997, *Hydrolog. Sci. J.*, 50(6), 949-961, 2005.
- 764 Juen, I., Kaser, G., and Georges, C.: Modelling observed and future runoff from a
765 glacierized tropical catchment (Cordillera Blanca, Perú), *Global Planet. Change*, 59,
766 37-48, 2007.
- 767 Kalnay, E., Kanamitsu, M., Kistler, R., Collins, W., Deaven, D., Gandin, L., Iredell, M.,
768 Saha, S., White, G., Woollen, J., Zhu, Y., Leetmaa, A., Reynolds, R., Chelliah, M.,
769 Ebisuzaki, W., Higgins, W., Janowiak, J., Mo, K.C., Ropelewski, C., Wang, J., Roy,
770 J., and Dennis, J.: The NCEP/NCAR 40-Year Reanalysis Project. *Bull. Amer.*



- 771 Meteor. Soc., 77, 437–471, 1996.
- 772 Kaser, G.: Glacier-Climate Interaction at Low-Latitudes, *J. Glaciol.*, 47(157), 195-204,
773 2001.
- 774 Kaser, G., and Osmaston, H.A.: *Tropical Glaciers*, 228 pp., Cambridge University Press,
775 New York, 2002.
- 776 L'hôte, Y., Chevallier, P., Coudrain, A., Lejeune, Y. and Etchevers, P.: Relationship between
777 precipitation phase and air temperature: comparison between the Bolivian Andes and
778 the Swiss Alps : Glacier shrinkage in the Andes and consequences for water
779 resources, *Hydrolog. Sci. J.*, 50(6), 989-997, 2005.
- 780
- 781 .
- 782 Mölg, T. Cullen, N. J., Hardy, D. R., Kaser, G. and Klok, L.: Mass balance of a slope glacier
783 on Kilimanjaro and its sensitivity to climate, *Int. J. Climatol.*, 28, 881–892, 2008.
- 784 Mölg, T.; Cullen, N. J.; Hardy, D. R.; Winkler, M.; and Kaser, G.: Quantifying climate
785 change in the tropical midtroposphere over East Africa from glacier shrinkage on
786 Kilimanjaro, *J. Climate*, 22, 4162–4181, 2009.
- 787 Nash, J. E., and Sutcliffe, J. V.: River flow forecasting through conceptual models Part I – A
788 discussion of principles, *J. Hydrol.*, 10, 282–290, 1970.
- 789 Oerlemans, J., Giesen, R. H., and van den Broeke, M. R.: Retreating alpine glaciers:
790 increased melt rates due to accumulation of dust (Vadret da Morteratsch,
791 Switzerland), *J. Glaciol.*, 55, 729-736, 2009.
- 792
- 793 .
- 794 Rabatel, A., Francou, B., Soruco, A., Gomez, J., Cáceres, B., Ceballos, J. L., Basantes, R.,



- 795 Vuille, M., Sicart, J.-E., Huggel, C., Scheel, M., Lejeune, Y., Arnaud, Y., Collet, M.,
796 Condom, T., Consoli, G., Favier, V., Jomelli, V., Galarraga, R., Ginot, P., Maisincho,
797 L., Mendoza, J., Ménégos, M., Ramirez, E., Ribstein, P., Suarez, W., Villacis, M.,
798 and Wagnon, P.: Current state of glaciers in the tropical Andes: a multi-century
799 perspective on glacier evolution and climate change, *The Cryosphere*, 7, 81–102,
800 doi:10.5194/tc-7-81-2013, 2013.
- 801 Radić, V., and Hock, R.: Regionally differentiated contribution of mountain glaciers and ice
802 caps to future sea-level rise. *Nature Geoscience*, 4(2), 91–94, 2011.
- 803 Rojas, M.: Multiply Nested Regional Climate Simulation for Southern South America:
804 Sensitivity to Model Resolution, *Monthly Weather Review*, 134, 2208–2223, 2006.
- 805 Sicart, J.-E., Hock, R. and Six, D.: Glacier melt, air temperature, and energy balance in
806 different climates: The Bolivian Tropics, the French Alps, and northern Sweden. *J.*
807 *Geophys. Res.*, 113, D24113, doi:10.1029/2008JD010406, 2008.
- 808 Urrutia, R., and Vuille, M.: Climate Change projections for the tropical Andes using a
809 regional climate model: Temperature and precipitation simulations for the end of the
810 21st century. *J. Geophys. Res.* **114**, D02108, doi:10.1029/2008JD011021, 2009.
- 811 Van den Broeke, M., Bus, C., Ettema, J., and Smeets, P.: Temperature thresholds for degree-
812 day modeling of Greenland ice sheet melt rates, *Geophys. Res. Lett.*, 37, L18501,
813 doi:10.1029/2010GL044123, 2010.
- 814 Villacis, M., Ressources en eau glaciaire dans les Andes d’Equateur en relation avec les
815 variations du climat : Le cas du volcan Antisana, PhD Thesis, Univ. Montpellier II,
816 Montpellier, France, 231pp., 2008.
- 817 Vincent, C. and D. Six. 2013. Relative contribution of solar radiation and temperature in
818 enhanced temperature-index melt models from a case study at Glacier de Saint-



- 819 Sorlin, France. *Annals of Glaciology*, **54**(63), 11–17.
- 820 Vuille, M., and Bradley, R.S.: Mean Annual Temperature Trends and Their Vertical Structure
821 in the Tropical Andes, *Geophys. Res. Lett.*, *27*(23), 3885-3888, 2000.
- 822 Vuille, M., Bradley, R.S., and Keimig, F.: Climate Variability in the Andes of Ecuador and
823 Its Relation to Tropical Pacific and Atlantic Sea Surface Temperature Anomalies, *J.*
824 *Clim.*, *13*, 2520-2535, 2000.
- 825 Vuille, M., Francou, B., Wagnon, P., Juen, I., Kaser, G., Mark, B.G., and Bradley, R.S.:
826 Climate change and tropical Andean glaciers: Past, present and future, *Earth-Sci.*
827 *Rev.*, *89*, 79-96, doi: 1144 10.1016/j.earscirev.2008.04.002, 2008.
- 828 Wagnon, P., Ribstein, P., Francou, B., and Pouyaud, B.: Annual Cycle of Energy Balance of
829 Zongo Glacier, Cordillera Real, Bolivia, *J. Geophys. Res.*, *104*(D4), 3907-23, 1999.
- 830 Wagnon, P., Lafaysse, M., Lejeune, Y., Maisinsho, L., Rojas, M., and Chazarin, J.P.:
831 Understanding and modelling the physical processes that govern the melting of the
832 snow cover in a tropical mountain environment in Ecuador, *J. Geophys. Res.*, *114*,
833 D19113, doi:10.1029/2009JD012292, 2009.
- 834 Winkler, M., Juen, I., Mölg, T., Wagnon, P., Gómez, J., and Kaser, G.: Measured and
835 modelled sublimation on the tropical Glaciar Artesonraju. *The Cryosphere*, *3*, 21-30,
836 2009.
- 837



838 **Table 1:** Equipment used. Sensors installed at AWS_{G1} station (for SEB calculations) and at
 839 AWS_{M1} at 4,900 m a.s.l. and their specifications; thermometers at AWS_{G2} (5,000 m a.s.l.)
 840 and at AWS_{M2} station (4,785 m a.s.l.) and rain gauge characteristics (4,550 m a.s.l.), and
 841 albedometer at AWS_{G3} (4,900 m a.s.l. on Glacier 12).

Data measured ¹	Type of sensor	Station name/elevation ² /type of surface	Period with data	Accuracy ³
Air temperature, °C	Vaisala HMP 45, aspirated ⁴	AWS _{G1} / 4,900 / Glacier	2000-2005, 2007-2008	±0.2°C
	Vaisala HMP 45, aspirated ⁴	AWS _{G2} / 5,000 / Glacier	2003-2004	±0.2°C
	Vaisala HMP 45, aspirated ⁴	AWS _{M1} / 4,900 / Moraine	2005-2008	±0.2°C
Air temperature, °C	Automatic HoboPro	AWS _{M2} / 4,785 / Moraine	2000-2008	± 0.2°C
Relative humidity, %	Vaisala HMP 45, aspirated ⁴	AWS _{G1} / 4,900 / Glacier	2000-2005	±2 %
Wind speed, m s ⁻¹	Young 05103	AWS _{G1} / 4,900 / Glacier	2000-2005	±0.3 m s ⁻¹
Wind direction, deg	Young 05103	AWS _{G1} / 4,900 / Glacier	2000-2005	±3 deg
Incident short-wave radiation, W m ⁻²	Kipp&Zonen CM3, 0.305<λ<2.8μm	AWS _{G1} / 4,900 / Glacier	1999-2005,2007-2008	±3 %
	Kipp&Zonen CM3	AWS _{G3} / 4,900 / Glacier 12	2006	±3 %
Reflected short-wave radiation, W m ⁻²	Kipp&Zonen CM3, 0.305<λ<2.8μm	AWS _{G1} / 4,900 / Glacier	1999-2005,2007-2008	±3 %
	Kipp&Zonen CM3	AWS _{G3} / 4,900 / Glacier 12	2006	±3 %
Incoming long-wave radiation, W m ⁻²	Kipp&Zonen CG3, 5<λ<50 μm	AWS _{G1} / 4,900 / Glacier	2002-2004	±3 %
	Kipp&Zonen CG3	AWS _{M1} / 4,900 / Moraine	2005	±3 %
Outgoing long-wave radiation, W m ⁻²	Kipp&Zonen CG3, 5<λ<50μm	AWS _{G1} / 4,900 / Glacier	2002-2004	±3 %
Daily precipitation, mm	Automatic Hobo Rain Gauge ⁵	P2 / 4,785 / Moraine	2000-2008	Opening: 200 cm ² Height: 100 cm
	Automatic Hobo Rain Gauge ⁵	P4 / 4,785 / Moorland	2000-2008	Opening: 200 cm ² Height: 100 cm

842 ¹Quantities are half-hourly means of measurements made at 15-s intervals except for wind direction, which are
 843 instantaneous values measured at 30-minute intervals.

844 ² m a.s.l.

845 ³according to the manufacturer

846 ⁴artificially aspirated to prevent over heating due to radiation.

847 ⁵Tipping bucket rain gauge, measured precipitation 0.214 mm by tipping.

848



849 **Table 2:** Data used in this study

Modeling	Period	Reference input data for modeling	Data gaps ¹	Data used to fill gaps ²	Model validation
PDD/Mass balance/Transient snowline	2000-2008	2000-2001: AWS _{G1}	2000-2001: 41%	AWS _{M2}	Measured mass balance & Melting boxes
		2002-2004: AWS _{G1}	2002-2004 : 14%	AWS _{G2} (otherwise: AWS _{M2})	
		2005: AWS _{G1}	2005: 21%	AWS _{M1} (otherwise: AWS _{M2})	
		2006: AWS _{M1}	2006: 13%	AWS _{M2}	
		2007-2008: AWS _{G1}	2007-2008: 8%	AWS _{M1} (otherwise: AWS _{M2})	

850 ¹Number of days with missing data (percent)

851 ²for wind speed, when data were missing at every station, we used NCEP1 reanalysis output



852 **Table 3:** Description of daily temperature data used and correlations with Antizana Glacier
 853 15 data at 4,900 m a.s.l. All the correlation coefficients are significant at $p = 0.001$.

Station	AWS _{G1}	AWS _{M1}	AWS _{M2}
Determination coefficient (r^2) with AWS _{G1} during each period ¹		Not available	0.80 (2002-2004)
Determination coefficient (r^2) with AWS _{G2} during each period ¹	0.90 & 0.85 (2002 & 2003)	0.87 & 0.89 (2005 & 2008)	0.75 & 0.86 (2003 & 2007- 2008)
Determination coefficient (r^2) with AWS _{M2} during each period ¹	0.80 (2002-2004)	0.89 (2005-2008)	

854 ¹Periods are in parentheses.



855 **Table 4:** Data used for basic model calibration and validation

856

Data	Model/method	Period	Location
Daily melting	SEB calculation	March 14, 2002-August 31, 2003 Jan – Nov 2005	AWS _{G1}
Measured melting	Melting boxes	March 12, 2002-June 11, 2003 (43 days): Antizana, (4,900 m a.s.l.)	AWS _{G1}
Terrestrial photographs	Automatic camera	2004–2008: 712 daily photos	Antizana Glacier 15 frontal moraine (4,875 m a.s.l.)
Daily albedo	Kipp & Zonen CM3 pyranometer	1999-2005: at AWS _{G1} 2006: on Antizana Glacier 12 (4,900 m a.s.l.) 2007-2008: at AWS _{G1}	On Antizana Glaciers 15 and 12

857

858



859 **Table 5:** Summary of the optimized sets of parameters with their respective modeling
860 scores, and sensitivity of parameters to $a_{\text{threshold}}$ variations in 2002-2003 and 2005.

Parameter	F_{ice}^1	F_{snow}^1	$T_{\text{threshold}}^2$	$a_{\text{threshold}}$	Measured ablation ³	Modeled ablation ³	R	RMSE ¹	E
Calibration on 2002-03	10.53	5.68	-2.05	0.49	11.3	11.0	0.81	6.5	0.64
Validation on 2005	10.53	5.68	-2.05	0.49	5.8	6.7	0.81	6.5	0.57
Calibration on 2005	9.45	4.24	-2.14	0.56	5.8	6.2	0.84	5.5	0.69
Validation on 2002-03	9.45	4.24	-2.14	0.56	11.3	10.4	0.8	6.8	0.62
Validation of mean parameters on 2002-03	9.99	4.96	-2.09	0.52	11.3	10.7	0.81	6.6	0.63
Validation of mean parameters on 2005	9.99	4.96	-2.09	0.52	5.8	6.4	0.83	5.9	0.64
Sensitivity in 2002-03	9.91	4.87	-2.14	0.56	11.3	11.1	0.79	6.3	0.63
Sensitivity in 2005	9.38	4.38	-2.05	0.49	5.8	5.7	0.82	5.7	0.67

861 ¹in mm w.e. °C⁻¹ d⁻¹

862 ²in °C

863 ³in m w.e.



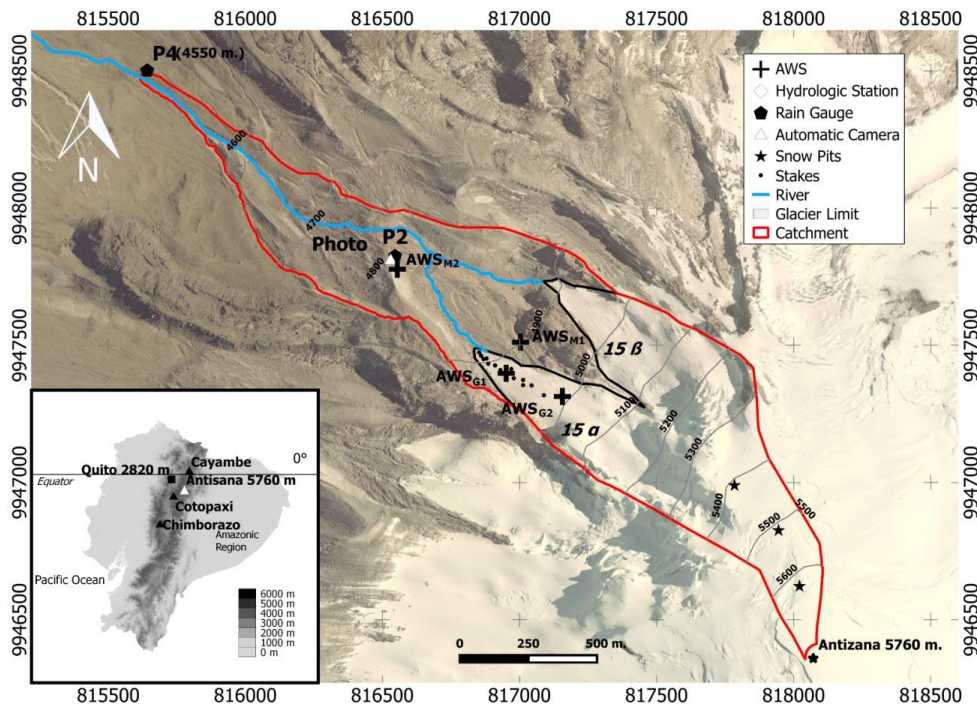
864 **Table 6:** Model sensitivity tests. Values (in m w.e. a⁻¹) are the differences between the
 865 “original” mass balance (0.08 m w.e. a⁻¹) and the mass balance resulting from the sensitivity
 866 test over the 2000-2008 period. Here, the “original” mass balance refers to the mass balance
 867 obtained with final parameters given in section 5.6, and the sensitivity test mass balance
 868 results from computations with the parameter value given in the same cell.

$T_{\text{Threshold}}$		F_{ice}		F_{snow}		$Lapse\ Rate$		$Sublimation$		$Precipitation$	
Value (°C)	difference	Value (mm w.e. °C ⁻¹ d ⁻¹)	difference	Value (mm w.e. °C ⁻¹ d ⁻¹)	difference	Value (°C km ⁻¹)	difference	Value (mm w.e. a ⁻¹)	difference	Value	difference
-2.14	-0.06	10.53.	-0.02	5.68.	-0.21	-9.2	0.08	Constant with elevation	0	-76%	-1.13
-2.09	0	9.99	0	4.96	0	-8.5	0				
-2.05	0.05	9.45.	0.02	4.24.	0.21	-8.2	-0.04	Linear decrease to 0 (summit)	0.13	0%	0

869



870



871

872 Figure 1: Orientation map of Antizana Glacier 15 showing location of monitoring

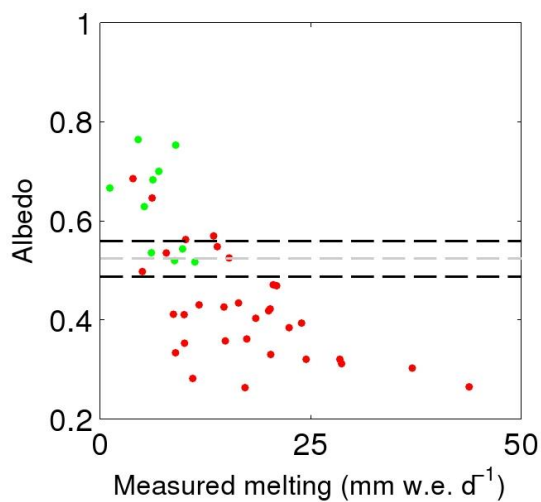
873 equipment. Projection is on UTM zone 17, coordinate system is WGS84. Inset is a physical

874 map of Ecuador. In this figure, AWS_{G3} is not shown. The background image is an

875 orthoimage of Antizana Volcano taken in 2010 by the *Instituto Geográfico Militar* of

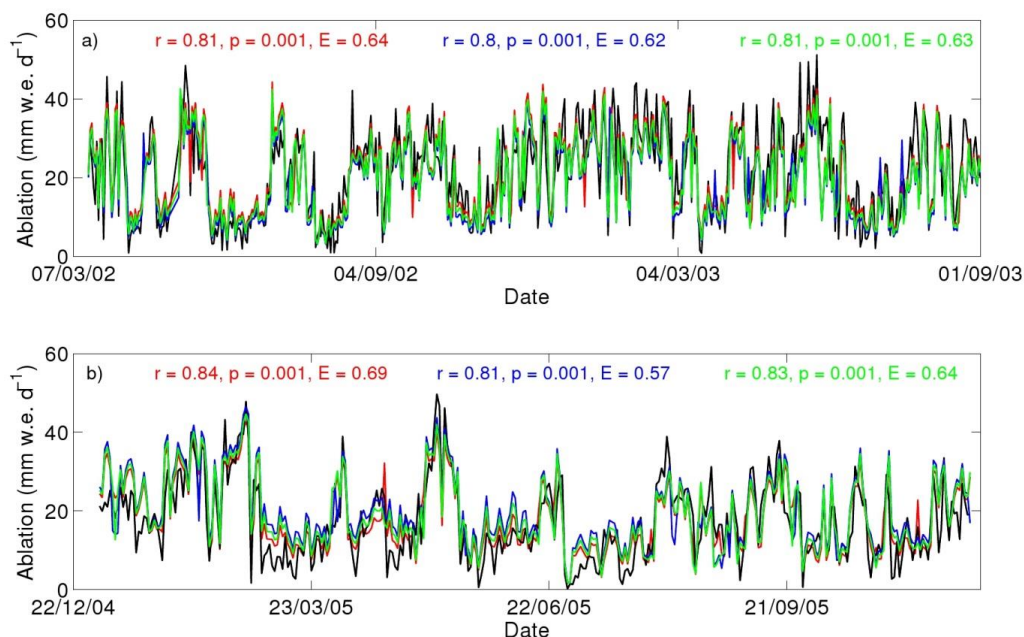
876 Ecuador: <http://www.geoportaligm.gob.ec/portal/index.php/catalogo-de-datos/>)

877

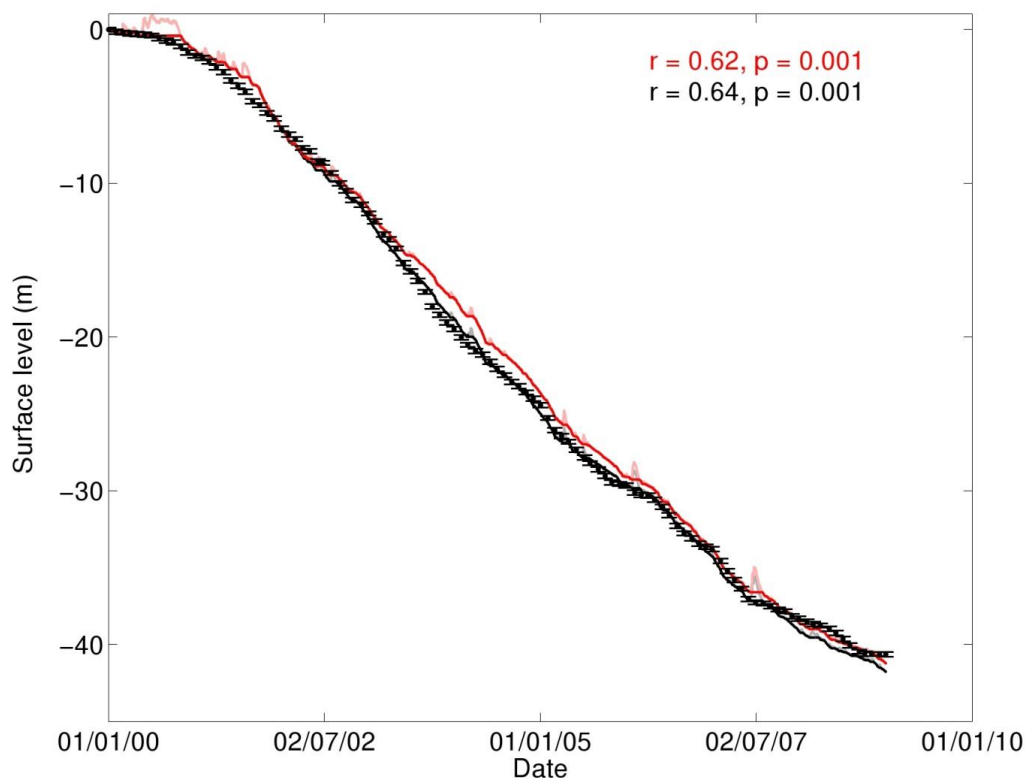


878

879 Figure 2: Comparison between measured melting rates in melt boxes and mean daily albedo
880 for snow (green) and ice (red). Dashed horizontal black lines are optimized thresholds
881 between snow, and ice for 2002-2003 ($a_{\text{threshold}} = 0.49$) and 2005 ($a_{\text{threshold}} = 0.56$). The
882 dashed gray line is the mean albedo threshold ($a_{\text{threshold}} = 0.525$).

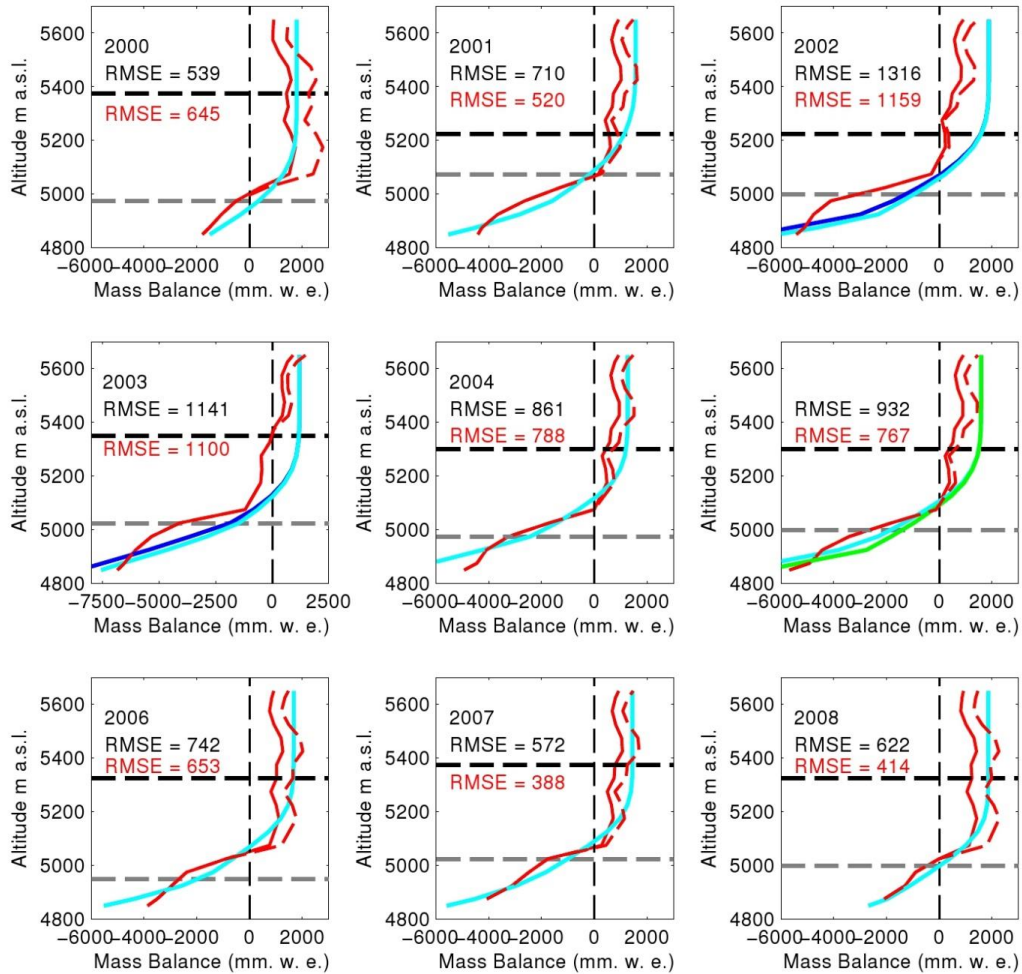


883
884 Figure 3: (a) Comparison between computed daily ablation rates obtained with the SEB
885 model (black) and with the basic model. The red curve is the optimized modeling for 2002-
886 2003, i.e. using parameters (F_{ice} , F_{snow} , $T_{threshold}$ and $a_{threshold}$) optimized on 2002-2003. The
887 blue curve is the validation curve using parameters optimized using 2005. The green curve is
888 the same as the red curve but accounts for the mean parameters given in section 5.4. (b)
889 Same as (a) but for 2005. The colors of the correlation coefficients correspond to those of
890 the curves.



891

892 Figure 4: Comparison between modeled (black and red lines) and measured (dots with error
893 bars) surface mass balance (in m of ice) at 4,900 m a.s.l. between 2000 and 2008. The gray
894 and pink lines represent the level of snow assuming a density of 200 kg m^{-3} . The red line is
895 the results of the basic model using the mean parameters given in section 5.6. The black line
896 shows the results using mean parameters given in section 5.6, except between March 15,
897 2002 and August 31, 2003, when the parameters given in section 5.1 were preferred, and
898 between January 1, 2005 and November 30, 2005 when the parameters given in section 5.3
899 were preferred. The correlation coefficients are between observed and modeled monthly
900 mass balance. The colors of the determination coefficients correspond to the colors of the
901 symbols.

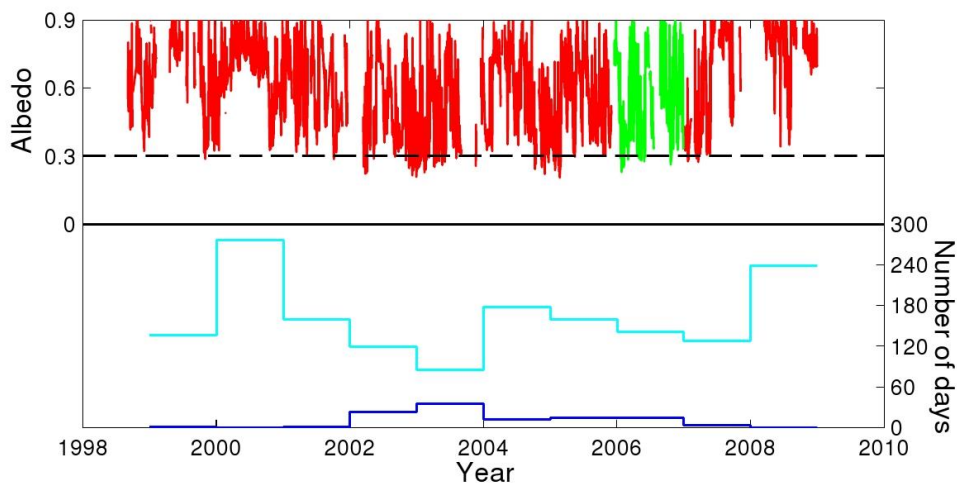


902

903 Figure 5: Variations in the point mass balance versus elevation for each year between 2000
 904 and 2008 assuming sublimation remains constant with elevation. The study year is given in
 905 the upper left corner of each panel. The continuous red curve is the measured mass balance;
 906 the dashed red line is accumulation multiplied by 1.6 as suggested by Basantes Serrano et al
 907 (2016); the light (dark) blue lines are modeled mass balance assuming model parameters are
 908 the mean coefficient given in section 5.6 (in section 5.1, respectively). The green line is the
 909 modeled mass balance assuming model parameters are the coefficient given in section 5.3.
 910 The horizontal dashed lines represent the elevation of the lowest accumulation measurement



911 (black) and of the highest ablation stake (gray) surveyed during the corresponding year.
912 RMSE is computed between observed and modeled mass balance at each elevation range.
913 Values in black are for $b(z)$ values given by Basantes Serrano et al (2016), values in red are
914 those obtained when accumulation is multiplied by 1.6.

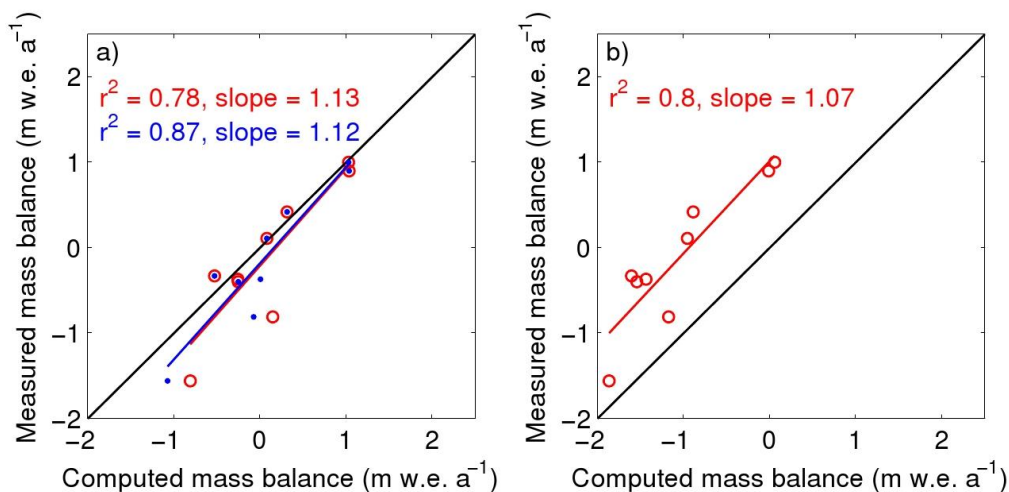


915

916 Figure 6: Daily albedo (upper panel) at 4,900 m a.s.l. on Antizana Glacier 15 (from 1999 to
917 2005 and in 2008, in red) and at 4,900 m a.s.l. on Antizana Glacier 12 (2006, green).
918 Missing data between December 17, 2001 and March 14, 2002 are not accounted for,
919 otherwise it would have increased the number of occurrences in 2002. Lower panel: The
920 dark blue line shows the number of days with albedo values below 0.3, the light blue line
921 shows the days with albedo values above 0.56.



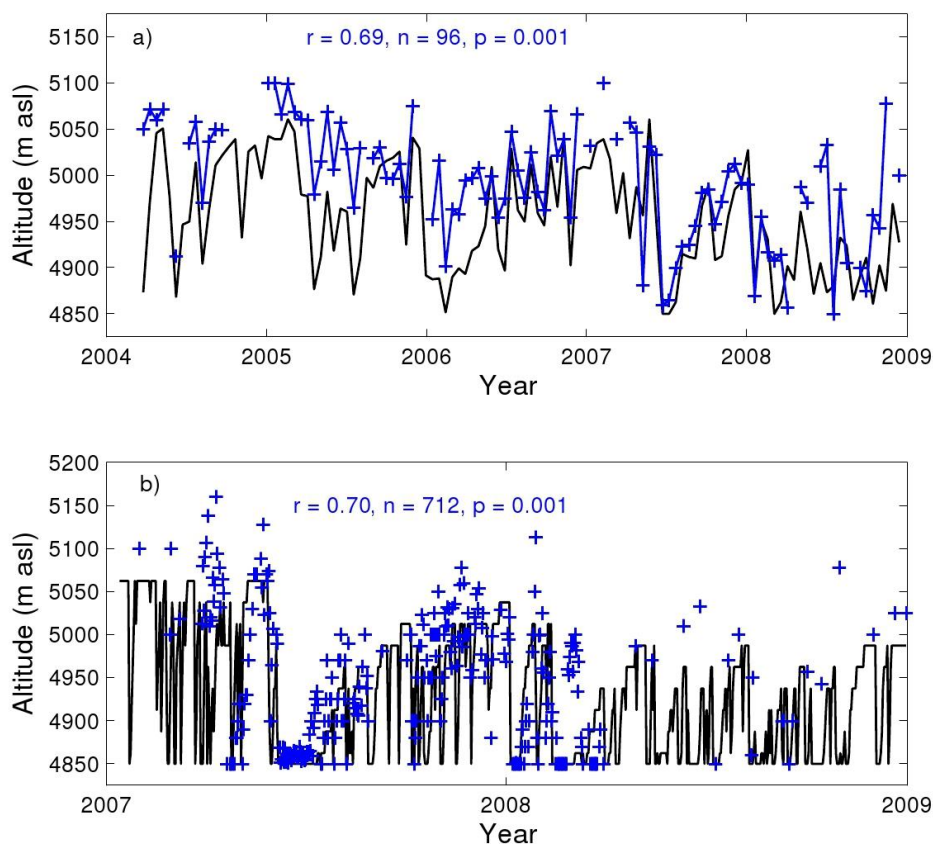
922



923

924 Figure 7: Comparison between the computed and the measured glacier-wide annual mass
925 balance of Antizana Glacier 15. (a) Modeled data are forced with temperature and
926 precipitation data from Antizana Glacier 15 catchment. Blue dots indicate the results using
927 the mean calibration parameters given in section 5.6. Red circles are the results using
928 optimized parameters given in section 5.6 except for 2002-03 and 2005 where parameters
929 come from section 5.1 and section 5.3 respectively. (b) Same as (a) but modeled mass
930 balance do not account for precipitation correction of 76% suggested by Wagnon *et al.*
931 (2009). The colors of the determination coefficient and slope values correspond to the
932 colors of the symbols. The 1:1 line is also shown in black.

933



934

935 Figure 8: Comparison between the observed (blue) and modeled (black) transient snowline
936 elevations accounting for a 76% increase in precipitation compared with measurements, at
937 (a) a 15-day time scale (15-day averages) over the period 2004-2008, and at (b) a daily time
938 scale over the period 2007-2008.